Journal of Materials Research and Technology 36 (2025) 5962–5977

Contents lists available at ScienceDirect

Journal of Materials Research and Technology

journal homepage: www.elsevier.com/locate/jmrt

Tribological characteristics of magnetorheological fluids based on carbonyl iron particles coated with various types of organosilanes

Michal Kocak [a], Sanjay Kumar [b], Miroslav Mrlik [c], Bharat Kumar [d], Chandra Shekhar [b], Rakesh Sehgal [e], M.F. Wani [b], Michal Kubik [f], Michal Sedlacik [a,c,*]

[a] Department of Production Engineering, Tomas Bata University in Zlín, 760 01, Zlín, Czech Republic
[b] Department of Mechanical Engineering, National Institute of Technology Srinagar, Hazratbal, Kashmir, 190006, India
[c] Centre of Polymer Systems, Tomas Bata University in Zlín, 760 01, Zlín, Czech Republic
[d] Centre for Automotive Research and Tribology, National Institute of Technology Hamirpur, Himachal Pradesh, 177005, India
[e] Department of Mechanical Engineering Department, National Institute of Technology Hamirpur, Himachal Pradesh, 177005, India
[f] Faculty of Mechanical Engineering, Brno University of Technology, 616 69, Brno, Czech Republic

ARTICLE INFO

Keywords:
Tribology
Friction
Wear
Magnetorheological fluid
Organosilanes

ABSTRACT

Magnetorheological fluids (MRFs) belong to the category of smart materials capable of reversibly altering their rheological behaviour under the influence of an external magnetic field. One of the most critical issues encountered in real-world applications, such as semi-active damping systems, is the long-term operational stability caused primarily by the excessive wear of the contact surfaces of the system. This study investigates the tribological and rheological behavior of magnetorheological fluids (MRFs) containing carbonyl iron particles (CIPs) coated with various organosilanes. The MRFs were prepared using CIPs coated with (3-aminopropyl) triethoxysilane (APTES), tetraethoxysilane (TEOS), vinyltrimethoxysilane (VTMS), and hexamethyldisilane (HMDS). Tribological experiments, conducted using a ball-on-disc configuration, demonstrated that organosilane-coated CIPs significantly improve the tribological characteristics compared to bare CIPs. The specific wear rate decreased from 3.393×10^{-4} mm^3 N^{-1} m^{-1} for bare CIPs to 1.248×10^{-4} mm^3 N^{-1} m^{-1} for HMDS-coated CIPs. The friction coefficient was also reduced, with HMDS-coated CIPs showing the lowest value. Rheological experiments revealed a direct correlation between shear viscosity and magnetic field strength, with organosilane-coated CIPs exhibiting lower viscosity and improved sedimentation stability. Among the coatings, HMDS showed the most significant reduction in wear and friction, attributed to the formation of a protective tribo-layer.

1. Introduction

A magnetorheological fluid (MRF) is a suspension typically composed of ferromagnetic spherical particles of carbonyl iron (CIPs) with a size range of 0.5–10 μm and high magnetic permeability. These particles are dispersed in a non-magnetic continuous phase [1,2]. Due to its properties, it is possible to alter the very nature of the rheological properties of MRF. It is classified among so-called smart materials, which have the ability to change and exhibit reversible characteristics as a result of a transformation from a liquid to an almost solid-like state. The application of an external magnetic field influences this change in rheological manner. Magnetorheological fluids (MRFs) in the off-state usually exhibit slightly non-Newtonian behaviour. However, for magnetorheological (MR) device modelling, the Newtonian behaviour of MRFs is usually assumed. As different values of a magnetic field are applied, the yield stress also linearly increases for low fields. The action of the magnetic field leads to a dynamic phase transition, where the magnetic particles, under the influence of an external magnetic field, form chain-like or clustered structures, thus altering the rheological properties of the suspension [3–8].

Recently, magnetorheological fluids have been used in various automotive, construction, and military industries. These systems are used in the form of damping systems [9,10]. One of the major problems limiting their operational stability is the high wear rate caused by friction of the contact surfaces. Several studies have already been conducted to address the issue of MRF's tribological properties. When evaluating

* Corresponding author. Department of Production Engineering, Tomas Bata University in Zlín, 760 01, Zlín, Czech Republic.
E-mail address: msedlacik@utb.cz (M. Sedlacik).

https://doi.org/10.1016/j.jmrt.2025.04.238
Received 24 February 2025; Received in revised form 10 April 2025; Accepted 22 April 2025
Available online 22 April 2025

the magnitude of wear, it is necessary to separate the effect of the frictional shear forces from the effect of interfacial particle slip. Sarkar and Hirani [11] presented the possibility of continuously controlling the magnetic field by modifying the tribological tester. The coefficient of friction (COF) scales with the magnetic field. Thus, MRFs exhibit a controlled change in tribological properties as the magnitude of the magnetic induction changes [12]. In a closer examination of the operational wear of the MRF system, the wear characteristics of the O-ring used in the dynamic system were investigated [13,14]. The COF between the O-ring and the piston rod increases with the particle size and mass fraction of the CIPs in the fluid. The abrasive action of the MRF particles on the O-ring surface is the main and most common cause of wear [13].

There are, however, some promising ways to obtain better mechanical properties for MRFs, especially with the modification of the CIPs. Bombard and de Vicente proved that the presence of an amorphous silica surface coating on some commercial CIPs can improve the antiwear properties and reduce the friction magnitudes. This fact also correlates with the CIPs size used in the suspension [15]. The approach of core-shell CIPs structures also exhibits optimized sedimentation stability properties, which is also one of the issues limiting long-term operational stability [16]. The synthesized CIPs exhibited lower shear stress without losing the MR properties of the suspension [17]. Sedimentation stability was also enhanced by adding a submicron layer of fumed silica to the MRF resulting in reduced sedimentation. This admixture also affects the flocculation stability with no noticeable change in the MR behaviour when the magnetic field is altered [18,19]. Eshgarf and co-workers [20] tested the modification of a suspension based on conventional CIPs by adding synthesized magnetite nanoparticles into the system. This modification was tested using a rotational rheometer, and the resulting analysis suggests that the magnetic nanoparticles increase the stability of the CIPs deposition and improve the magnetorheological properties. Another element affecting the tribological behaviour of the MRFs is the use of lubricants. A study focusing on the tribological behaviour of ferrofluid lubricated MRF was conducted during the both on and off-state. The results indicated a lower COF for the MRF containing the lubricant than the standard MRF, which correlates with less wear damage [21]. The lubrication film formed between the particles and plates reduced abrasion by creating a protective layer on the surface. Using a film with poorer lubrication properties resulted in higher yield stress and greater susceptibility to shear thickening, leading to a deterioration of the tribological and the MR properties [22].

The size and shape of the particles are another aspect that can have significant influence on the stability of the MR suspension and the magnitude of wear [23]. A study by R. Upadhyay [24] investigated the effect of CIP's shape on the properties of MRF. The use of iron flake particles showcased several advantages over spherical particles. Their shape allowed for a reduction of the friction between the particles and thus improving the properties. Furthermore, the flakes had a larger surface area, which increased their ability to interact with the magnetic field and thus elevated the magnetic response of the whole system. The flake-shape typology also tends not to settle, which improved the sedimentation of the overall suspension. Although very promising results were obtained using magnetic flakes compared to spherical particles [25,26], and further research into the use of different morphologies to improve the tribological properties of MRFs is certainly worthwhile, spherical CIPs constitute the vast majority of dispersed magnetic particles in MRFs (easy and mass production). Therefore, further investigation into improving the tribological properties of CIP-based systems is also warranted, which is the essence of this work. The surface typology of the dispersed particles also played an important role in the experiment, where the surface of the CoNi microsphere was modified using carbon quantum dots. This modification led to the formation of a rough surface, which played an important role in the determination of the tribological properties. The microspheres of CoNi with rough surfaces improved the tribological properties of the MRF. These results suggested that the rough surface of the CoNi microspheres could positively influence the magnetorheological effect [27]. Coating CIPs with silver nanoparticles can also indeed help prevent abrasion [28,29]. Silver nanoparticles provide a protective layer that can enhance the tribological properties of the particles, reducing wear and friction. The implementation of the MRF studies for braking performance testing is one of the next steps to develop fine-tune smart systems for future applications. The results of the MRF study enriched with graphite flakes confirmed that this modification influences reducing brake rotor wear. These measurements were performed using a full-scale brake inertial dynamometer, which allowed testing only the wear under real conditions [30]. Further practical studies investigated the thermal and tribological properties of a disc MR brake system operating in shear mode under different operating conditions. The test results showed that the small working limit significantly affected the abrasion properties of the brake system, which was manifested by large ridges and deep grooves on the worn surfaces of the friction pads [31]. In tribological applications, organosilanes play a critical role in reducing the COF and wear [32]. Juretzka et al. explored the tribological and tribochemical behavior of organosilane as oil additives, reporting that these compounds form tribofilm during tests with mineral oil lubrication. This process leads to the development of a multilayer film, which significantly enhances tribological performance and corrosion resistance. In another study, Satyanarayana et al. [33] investigated the tribological effects of octadecyltrichlorosilane (OTS) and 3-aminopropyltrimethoxysilane (APTMS) monomolecular layers. Their findings revealed a significant reduction in COF with the use of OTS, while APTMS led to an increase in COF. The study concluded that a composite layer of self-assembled monolayers could be more effective in improving the wear resistance of MEMS components.

This study focuses on expanding the current knowledge of tribology in the field of MRFs. To this end, an experiment was conducted to compare the COF in MRF with modified CIPs coated with an organosilane layer. This type of coating was chosen primarily because it does not suppress magnetic properties, allowing the formation of chains during measurements under the influence of an external magnetic field. Particles coated with (3-aminopropyl)triethoxysilane (APTES) exhibit lower magnetic saturation, yet they retain sufficient magnetic attraction for separation purposes [34]. APTES also generally enhances particle dispersion in the carrier fluid and provides anti-corrosion protection [35,36]. Another organosilane demonstrating excellent tribological properties is tetraethoxysilane (TEOS). This film reduces COF and significantly decreases the wear rate [37]. CIPs coated with (3-amino--propyl)triethoxysilane (APTES), tetraethoxysilane (TEOS), vinyltrimethoxysilane (VIN), and bis[3(3-methoxysilan)propyl]amine (BIS) were found to exhibit higher MRF stability than uncoated particles, suggesting that the coating influences MRF stability [38]. Another study examining the functionality of organosilane coatings in terms of wear and COF involves the use of 1,8-bis(triethoxysilyl)octane and 1H,1H,2H,2H-perfluorooctyltriethoxysilane coatings, as well as their combination, to improve anti-adhesion properties during demolding. The combination of these coatings reduces COF by up to 30 % compared to a single-layer coating [39]. Hexamethyldisilane (HMDS), used as a precursor for SiCN film deposition, was also investigated in a study examining the film's effect on COF. HMDS proved to be an effective material for improving the mechanical and tribological properties of films, leading to a lower COF and better wear resistance compared to other types of films, such as SiC films [40]. In another study, HMDS films synthesized at 300 °C with higher self-bias voltages exhibited strong adhesion, increased hardness (up to 19 GPa), and a low coefficient of friction (~0.2). The films demonstrated excellent wear resistance. These properties make them promising candidates for protective coatings in tribological applications [41]. Based on previous studies, it can be assumed that the presence of an organosilane coating reduces COF and wear of contact surfaces without compromising magnetic response.

An experiment was designed in this study to compare the COF in

MRFs containing modified organosilane-coated CIPs. The tribological properties were assessed under varying magnetic field strengths, and the relationship between the magnetic field magnitude and the minimal wear of steel-on-steel point contact surfaces was examined.

2. Experimental

2.1. Materials

Carbonyl iron particles (ES grade, 6 μm in diameter, spherical particles with iron content >99.5 %) were used as the magnetic agents in the MRFs under investigation and were purchased from BASF (Germany). Hydrochloric acid (HCl, 35 %, p.a.) was used for cleaning and the activation of CIP's surface. Toluene (ACS reagent, ≥99.5 %) was used as a silanization carrier as well as for particle washing. Dimethyl sulfoxide (ACS reagent, ≥99.9 %) was used as an alternative silanization carrier. Acetone (ACS reagent, ≥99.5 %) and ethanol (denatured with about 1 % methyl ethyl ketone) were used for particles washing. All these chemicals were purchased from Penta Labs (Czech Republic). For the CIPs modification, (3-aminopropyl) triethoxysilane (3APTES, ≥99 %), tetraethoxysilane (TEOS, ≥98 %), vinyltrimethoxysilane (VTMS, ≥97 %), and hexamethyldisilane (HMDS, ≥99 %) were used individually as silane agents and were acquired from Sigma Aldrich (MO, USA).

2.2. Modification of particles with various organosilanes

The CIPs (100 g) were first washed with 0.1 M HCl to purify them out of various oxidized residues created during storage. Then, the particles were washed 3 times with 100 mL of distilled water, ethanol and acetone and dried under a vacuum atmosphere (100 mbar) at 30 °C overnight. In order to create the organosilane layer on the surface of CIPs, the washed and cleaned particles were modified according to the following procedure:

The CIPs (25 g) were dispersed in the toluene (100 mL) placed inside of a two-neck round bottom flask. The reaction mixture was bubbled for 10 min under argon atmosphere. A vigorous stirring was established with a mechanical stirrer at 500 rpm. The various silane agents (6 mL) (3APTS, TEOS and VTMS) were added dropwise and homogenized for 60 min. The whole mixture was heated up to 110 °C containing a condenser and it was refluxed for 8 h. The particles were washed 3 times with toluene (100 mL), ethanol (100 mL), and acetone (100 mL). The modified particles were pre-dried in ambient atmosphere for 2 h at 60 °C followed by vacuum drying at 30 °C and 100 mbar overnight. Lastly, the Particles were ground using a mortar dish to obtain a fine powder.

The modification of the CIPs surface with HMDS was, however, due to the different nature, carried out with the following procedure: The CIPs (25 g) were immersed in DMSO (100 mL), and 6 mL of HDMS was added dropwise under vigorous stirring. The reaction was set up under a condenser, temperature 160 °C, and decreased vacuum. The cooling system at the condenser was ethylene glycol, and the mixture was cooled down to 8 °C to achieve reflux. The washing procedure was the same to as for the previously mentioned organosilanes; however, DMSO was used in the first step. The particles were dried and ground as the other CI-organosilane systems.

2.3. Particles characterization

The successful modification of CIPs with the organosilanes was analysed by following the literature [38]. Moreover, the FTIR investigations have been performed using Nicolet FT-IR spectrometer (Nicolet Magna-550 Spectrometer, USA) in the region of 4000–600 cm^{-1} on the neat CIPs and their modified analogues. The magnetic properties of the modified particles were investigated using vibrating sample magnetometry (VSM, 7407, Lakeshore, USA). In a typical measurement, 250–300 mg of the particular sample was placed in the cuvette. The wide range of the magnetic fields from −10 000 Oe to 10 000 Oe was applied and magnetization saturation was obtained. All measurements were performed under laboratory temperature. In order to investigate the thickness of the created coatings on the surface of CI particles the Langevin model have been used to calculate the magnetic core diameter which was already applied at various studies [42,43].

$$M(H) = \left[\frac{1}{\tanh\left(\frac{m\cdot\mu_0\cdot H}{k\cdot T}\right)} - \frac{1}{\frac{m\cdot\mu_0\cdot H}{k\cdot T}}\right]\cdot M_S \quad (1)$$

where m is the magnetic moment, μ_0 is the magnetic permeability of free space ($4\pi \times 10^{-7}$ H m^{-1}), H is the magnetic field, k is the Boltzmann constant (1.38×10^{-23} J K^{-1}), T is the temperature in Kelvin, and M_s is the saturation magnetization.

Under the assumption of the spherical shape of particles, the magnetic particle diameter, d, was determined by the following relation:

$$d = \left(\frac{6\cdot m}{\pi\cdot M_S}\right)^{\frac{1}{3}} \quad (2)$$

2.4. Magnetorheological analysis

In total, five MRFs of the same concentration of CIPs (60 wt%) in silicone oil (viscosity 350 cSt, Sigma Aldrich) were prepared. Their coding corresponds to the type of organosilane used (e.g. MRF-TEOS corresponds to an MRF containing CIPs modified with tetraethoxysilane, MRF-ES contains bare CIPs). The MRFs were prepared by thoroughly mixing the corresponding amount of CIPs in silicone oil. Prior to use, the given MRF was homogenized/stirred for 5 min by hand with a glass rod and then for 1 min using ultrasound.

The magnetorheological performance of the MRFs was investigated using a rotational rheometer Physica MCR 502 (Anton Paar GmbH, Austria) with an MRD 170/1 T magneto-cell at 25 °C. A parallel-plate measuring system with a diameter of 20 mm and a gap of 0.5 mm was used. Magnetosweep experiments were perform to investigate the MRF's response to magnetic fields. Firstly, the MRF was mixed at a shear rate of 50 s^{-1} for 1 min without the presence of a magnetic field. Then, the current in the magneto-cell was linearly increased within the interval 0–0.65 A (magnetic field intensity 0–200 kA m^{-1}) in the time interval of 80 s and at a constant shear rate of 10 s^{-1} (40 of measured points). The rheological measurements were repeated three times for each MRF. For this type of measurement, the error bars are not higher than the actual size of the symbol in Fig. 5. The sedimentation stability of prepared samples was measured using visual observation technique.

2.5. Tribological experiments

A multifunctional universal tribometer (R-tech, MFT-5000) was used for performing the tribological experiments using a reciprocating drive with or without the application of a magnetic field as shown in Fig. 1. The disc specimen was mounted on the reciprocating drive using a proper fixture, while the ball was fixed to the upper ball holder. The upper surface of the disc was submerged in MRF. The tests were conducted under boundary lubrication conditions [44,45], the detailed calculation for which is shown in the Supporting information. Similarly, on the basis of Eqs. (3)–(6), the lambda parameter of 0.40, 0.35, 0.25, 0.62 and 0.47 was obtained for MRF-ES, MRF-3APTS, MRF-HMDS, MRF-TEOS and MRF-VTMS, respectively. For all the conditions considered in this study, λ was less than 1, which conformed with the boundary lubrication regime. A Neodymium permanent magnet was positioned below the disc, producing magnetic flux, as illustrated in Fig. 1.

The magnetic flux was quantified using a digital Gauss meter (DMG-102) and the magnetic field was not homogeneous throughout the sample. It varied with the radius of the disc, where a magnetic field of 5 mT was obtained in the centre of the disc and less (4.8 mT and 4.9 mT)

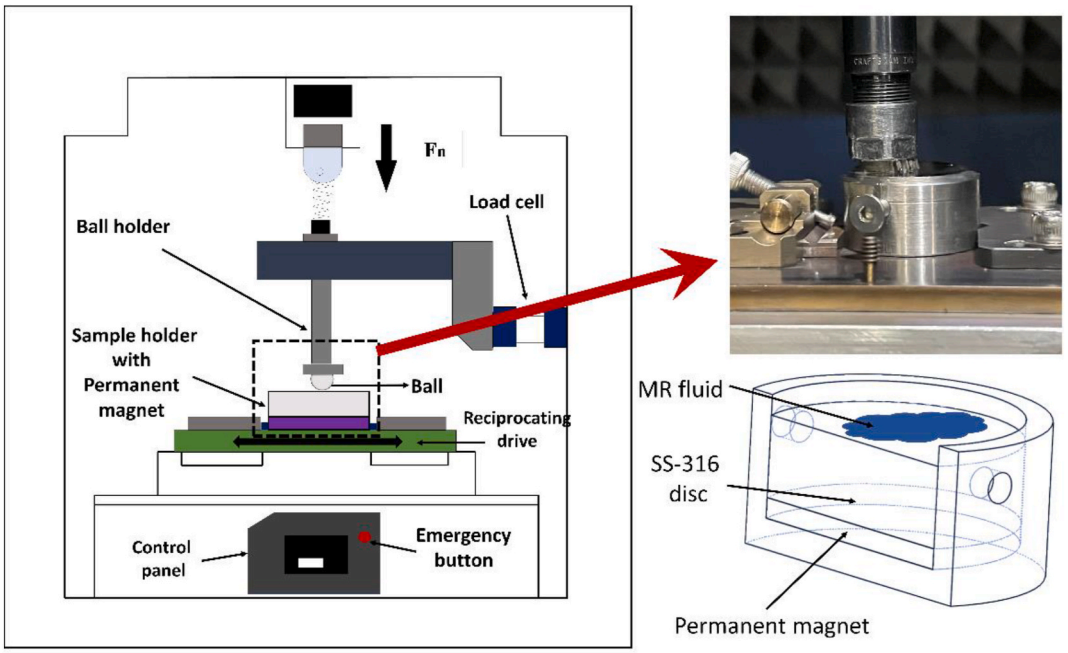

Fig. 1. Schematic image of universal tribometer with the setup of the holder.

Table 1
Parameters for tribological experiments.

Description	Value
Load (N)	15
Frequency (Hz)	10
Cycles	12500
Temperature	Room temperature
Magnetic field (mT)	5
MRF type	(MRF-ES), (MRF-3APS), (MRF-HMDS), (MRF-TEOS), (MRF-VTMS)

was found on the outer side of the disc. So, all tests were conducted in the centre region of the disc in this work. The ball and disc employed for the tribological experiments were comprised of stainless steel (SS-316).

$$h\,\mathrm{min} = 7.43\mathrm{R}\left(1 - 0.85e^{-0.31k}\right)\left(\eta u/E'R\right)^{0.65}\left(L/R^2E^*\right)^{-0.21} \quad (3)$$

$$E^* = \frac{2}{\frac{1-\nu_a{}^2}{E_a} + \frac{1-\nu_b{}^2}{E_b}} \quad (4)$$

$$\sigma^* = \sqrt{\left(\sigma_a{}^2 + \sigma_b{}^2\right)} \quad (5)$$

$$\lambda = \frac{h_{min}}{\sigma^*} \quad (6)$$

where:

u is the sliding velocity (m/s), k is the parameter of ellipticity, η *is* the absolute viscosity (Pa s), L is the Normal load (N), Rb is the radius of the flat disc (infinite), Ra is the ball's radius, ν_a is the Poisson's ratio for the ball material, ν_b is the Poisson's ratio for the disk material, Eb is the modulus of elasticity for the disk material (GPa), Ea is modulus of elasticity for the ball material (GPa). R is the effective radius of curvature, E^* is the equivalent modulus of elasticity of the tribopair, and σ^* is the equivalent surface roughness. σ_a and σ_b represent the surface roughness of the ball and disc, respectively. h_{min} denotes the minimum film thickness.

The samples were polished using various grits of emery papers (400, 800, 1000, 1200, 1500, and 2000). To achieve a mirror-like surface finish, a diamond paste within the range of 2 to 0.25 μm was applied to the samples and the polishing was performed with a velvet cloth. The tribological experiments were performed according to the ASTM standard G133-05 and the details of experimental parameters are listed in Table 1.

For each experiment, 2 mL of the MRF were used. Before and after each test, the specimens were cleaned with acetone and subsequently dried in an oven. The COF on the contact surfaces was assessed with and without the magnetic field. A 3-D profilometer (R-Tech, USA) was employed to examine the profile of the worn surfaces. The surface topography was examined using FE-SEM (Gemini-500, ZEISS, Germany) and EDX (EDX, Ametek) before and after each experiment.

3. Results and discussion

3.1. Particles characterization

In order to specifically confirm the presence of the various silanes' moieties on the surface of the CIPs, the FTIR investigations have been performed and the spectra are present in Fig. 2. In all cases, the presence of the vibration of C–H groups are clearly visible in grey rectangle which corresponds to the absorption bands from 3000 to 2800 cm^{-1}. Moreover, the presence of silane absorption bands from 1200 to 1100 cm^{-1} is apparent for all investigated samples. The individual absorptions of the specific moieties can be seen in Fig. 2a, where for CI-APTES, the C–N absorption band is in 1449 cm^{-1} and for the C–O stretching at 1185 cm^{-1} similarly as was already published [46]. The presence of TEOS on the CIPs surface was confirmed by typically seen absorption bands at 973 cm^{-1} for Si–OH, which is slightly lower than usual due to the covalent attachment to CIPs. Another absorption band is visible at 1488 cm^{-1} which is typical for C–H bending specifically visible at TEOS structure. The presence of the VTMS moiety was confirmed by a significant peak at 1654 cm^{-1}, corresponding to the C═C bond as a part of

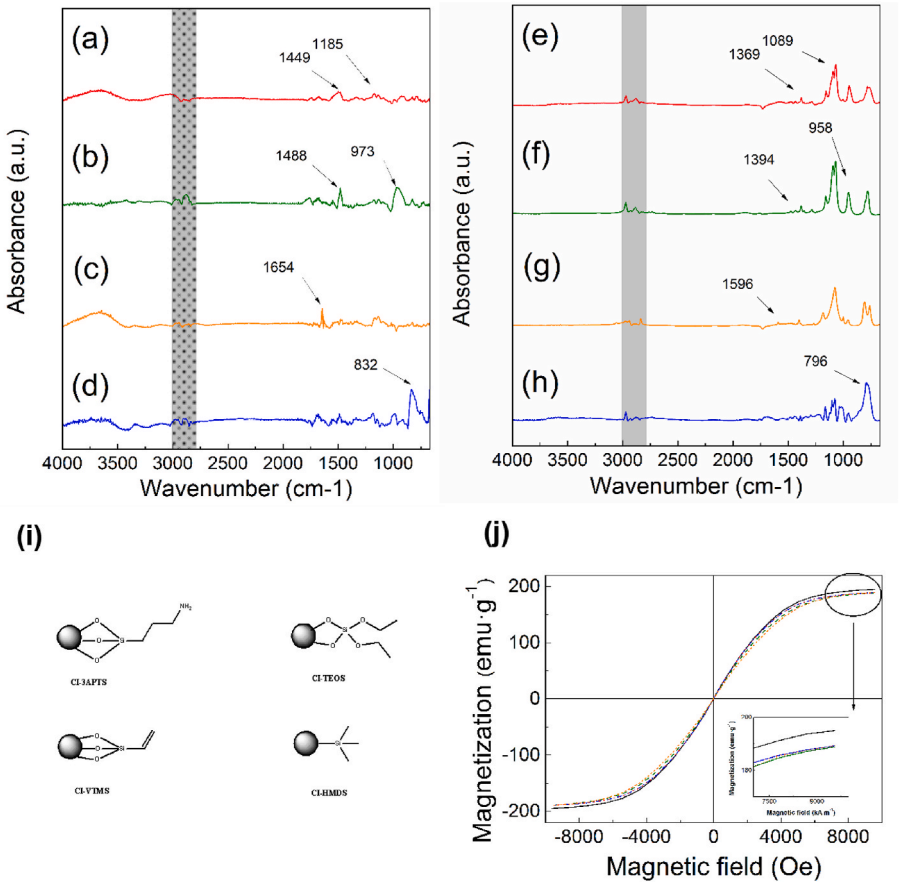

Fig. 2. FTIR spectra of various CIPs correspond to (a) CI-APTES, (b) CI-TEOS, (c) CI-VTMS and (d) CI-HMDS, and the corresponding starting organosilanes used for modification of CIPs (e–h). Schematic illustration of the CIPs surface modification using various organosilanes (i) and magnetization curve for CI-ES (black solid line), CI-3APTS (red dot line), CI-HDMS (blue dash-dot line), CI-TEOS (olive dashed line) and CI-VTMS (orange short dashed line).

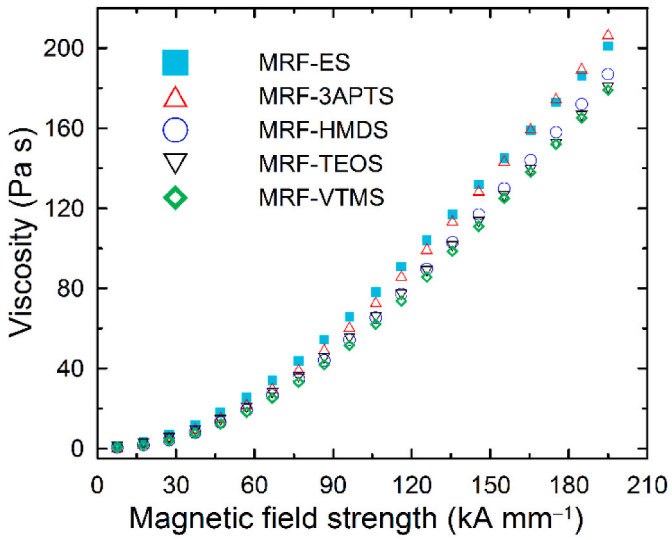

Fig. 3. Magnetosweep for the MRFs under investigation.

VTMS. The HMDS has typical band as other silanes, although due to the absence of Si–O bonds some of the peaks are missing. However, a significant peak at 832 cm^{-1} confirms the presence of the Si–C bond which is in majority present in this substance. The neat CIPs were not added to this figure, due to the fact, that they do not show any significant absorption peaks in the whole investigated range as was already published [47]. The corresponding neat silanes have slightly lower wavenumbers compared to CI-modified particles (Fig. 2e–h) which is a consequence of the modification and slight change in the structural difference between the original silane and after modification.

A schematic illustration of the particular bonding onto the CIPs surface is presented in Fig. 2i. In the case of the (3APTS, TEOS and VTMS) the synthesis procedure allows to creation of Si–O–C bond similarly as in the previously reported article [38]. Another synthesis was approach realized in case CI-HMDS particles under specific conditions of Si–C bond created due to the fact that such bond needs more energy similar as was published elsewhere [48].

The magnetization curve in Fig. 2j provides a clear evidence that neat CI particles have very good performance for intended application and are in good agreement with previous reports [42]. After the modification with silane-based moieties, the magnetization saturation has slightly decreased from 195 emu g^{-1} for neat CI to 189 emu g^{-1} similarly to our previous study [38], providing particles with sufficient magnetic capability for MR applications.

3.2. Magnetorheology

To demonstrate the magnetorheological effect of the studied MRFs, a magnetosweep was performed, during which the increase of viscosity of the MRF is monitored with the increasing intensity of the applied magnetic field (Fig. 3). Evidently, all studied MRFs show a significant MR effect as the dispersed magnetized microparticles (under the action of an external magnetic field) are connected into chain-like internal structures oriented along the magnetic field streamlines.

This phenomenon is macroscopically manifested by an increase in

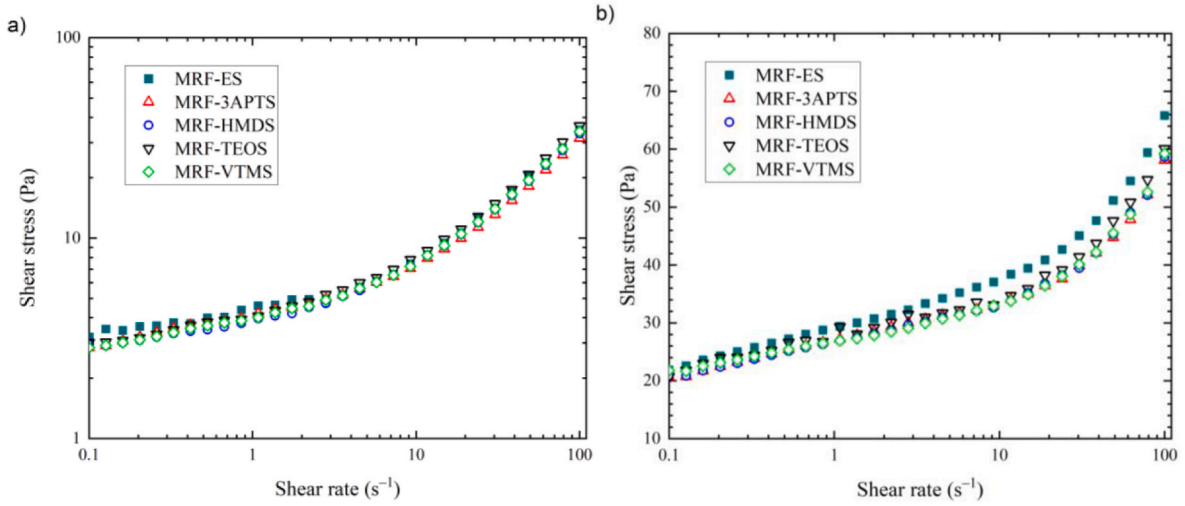

Fig. 4. Flow curves for the MRFs under investigation in the (a) off-state and (b) on-state (5 mT).

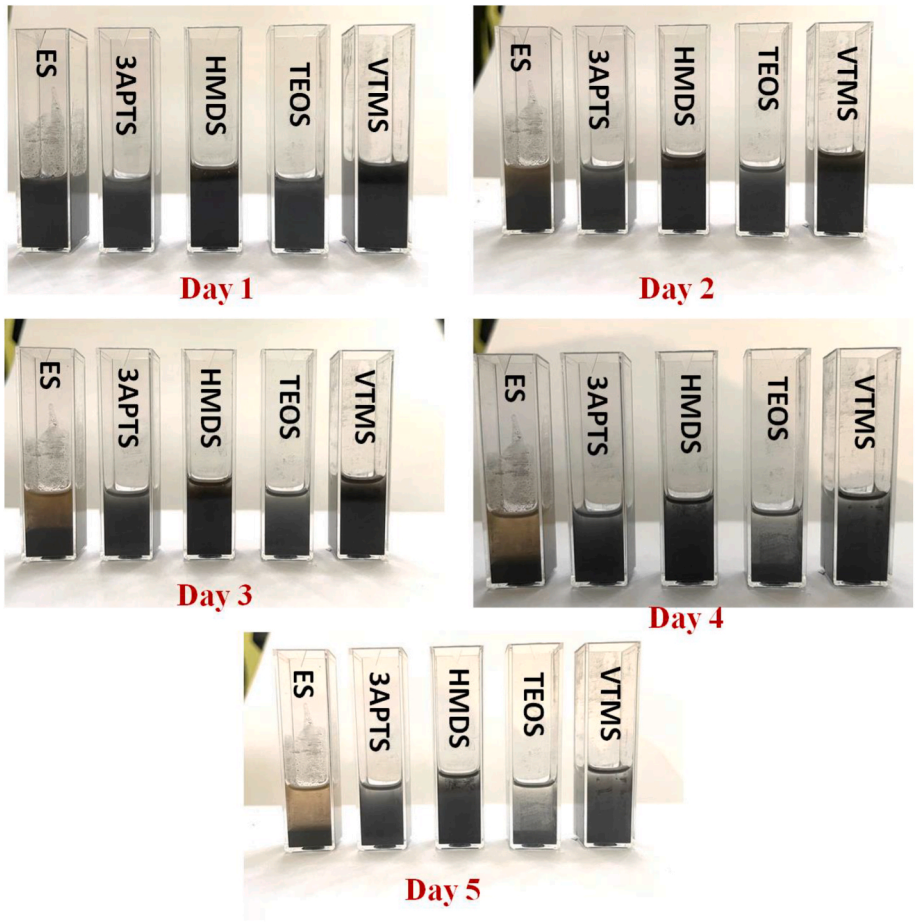

Fig. 5. Sedimentation stability test for five days.

viscosity corresponding to the intensity of the applied magnetic field. As can be seen in Fig. 3, MRF-ES exhibits the most significant MR effect at lower magnetic field intensities, which MRF-3APTS however exceeds at higher values of magnetic field intensity. This may be a consequence of the better wettability of the modified particles by the silicone oil used as a carrier liquid and more compact clusters not containing agglomerates (as may be the case with bare ES particles) in the presence of higher magnetic field intensities [49]. However, the MRFs with various organosilane-coated CIPs generally show a lower MR effect due to the lower permeability of organosilane-modified CIPs variants caused by the non-magnetic coating on the surface of the particles [38]. However, it is worth noting that the mentioned decrease in the MR effect is negligible and can only be observed when using linear scaling in Fig. 3.

Fig. 4a and b represent flow curves in the off-state and on-state (20 kA m^{-1}, which is ~ 5 mT for the magneto-cell and CI particles used), respectively, when in the absence of an external magnetic field, the

MRF-ES system exhibits the highest shear stress (i.e. also viscosity), which confirms the aforementioned fact that this suspension contains agglomerates, which are gradually disturbed with the increasing shear rate. All other systems formed by modified CIPs show lower shear stress at low shear rate values, which confirms the improved compatibility of particles with silicone oil due to the presence of an organosilane layer on the surface of the magnetic particles. Furthermore, when an external magnetic field is applied (Fig. 4b) with a magnetic flux density of 5 mT (identical to that used in tribological measurements), the MRF-ES exhibits slightly higher MR effect due to the highest magnetization of the particles, which corresponds to the course of the magnetosweep (Fig. 3).

3.3. Sedimentation stability

A 5-day sedimentation stability test was conducted on all prepared samples as shown in Fig. 5. The results showed that the ES-type particles exhibited poor sedimentation stability after just one day. In contrast, the organosilane-coated particles demonstrated significantly better sedimentation stability. This improvement can be attributed to the reduced bulk density of the organosilane-coated CIPs, which minimizes the density mismatch between the base fluid and the coated CIPs. Among the organosilane-coated samples, the MRFs based on TEOS and 3APTS-coated CIPs showed slightly lower sedimentation stability compared to those with HMDS and VTMS-coated CIPs. By the fifth day, all suspensions had settled and displayed similar sedimentation stability. Overall, the organosilane-coated CIPs-based MRFs outperformed the bare (ES) CIPs-based MRFs in sedimentation stability.

3.4. Tribological characteristics of prepared MRF

3.4.1. Coefficient of friction (COF) analysis

Fig. 6 illustrates the average COF of the samples (MRF-ES, MRF-3APTS, MRF-HMDS, MRF-TEOS, MRF-VTMS) and variation of the COF with sliding time in the presence and absence of the magnetic field. In the absence of a magnetic field, the avg. COF experienced a substantial reduction for both fluid types, whether comprising bare CIPs (MRF-ES)

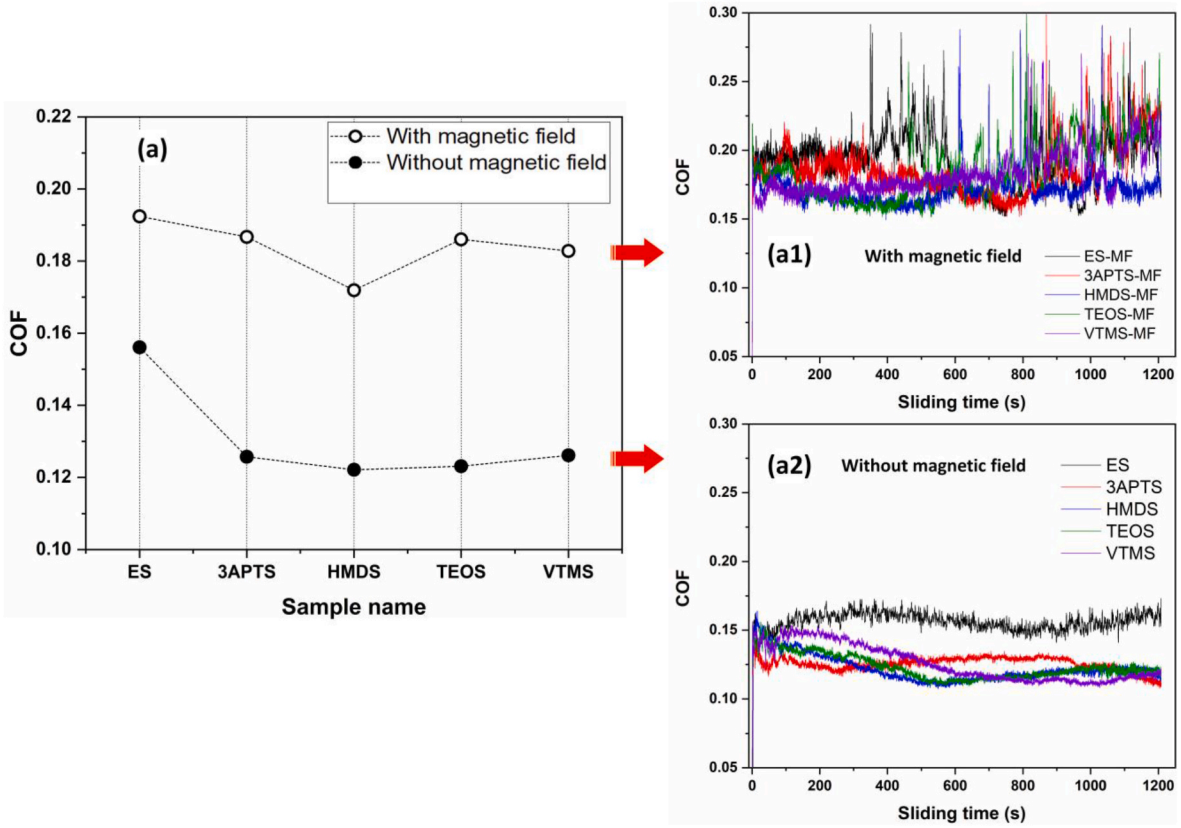

Fig. 6. (a) average COF over the entire time span graph of all the samples, (a1) COF as a function of sliding time graphs with the magnetic field (5 mT), and (a2) COF as a function of sliding time graphs without the application of magnetic field.

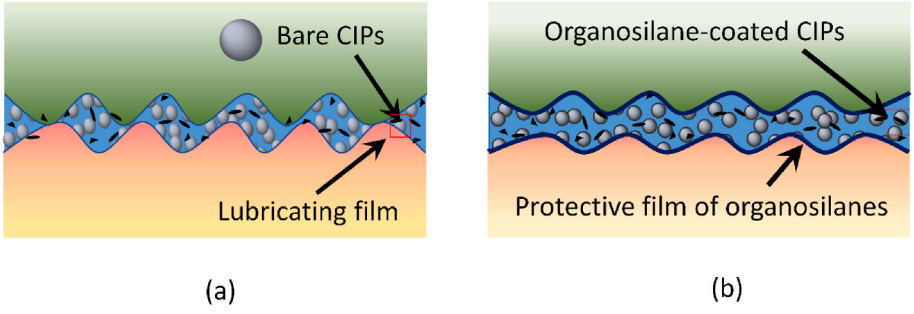

Fig. 7. Schematic of the lubrication mechanism of prepared MRFs (a) bare CIPs based MRF and (b) organosilane-coated CIPs based MRF.

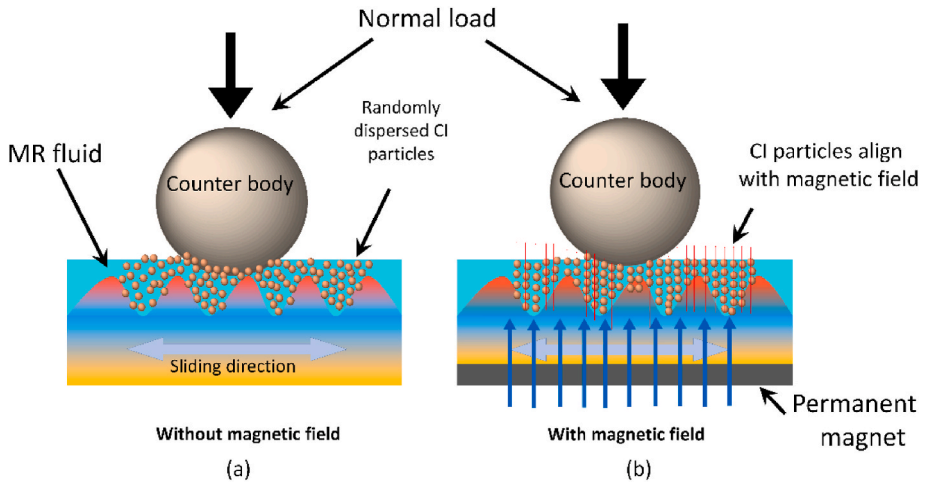

Fig. 8. Schematic of contact interface mechanism (a) magnetic field off, and (b) magnetic field on.

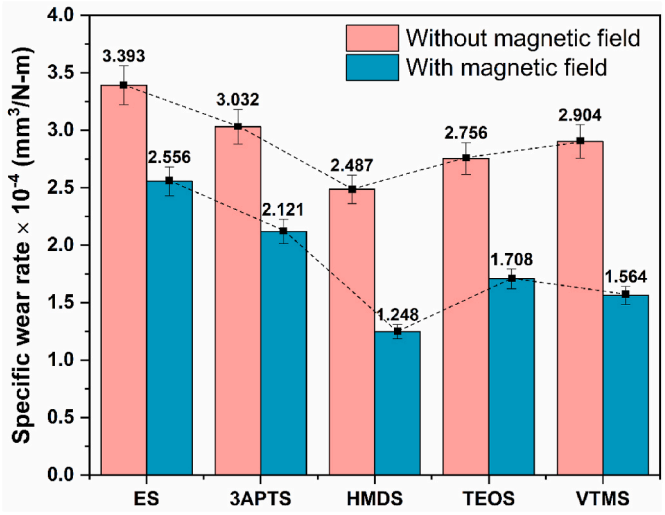

Fig. 9. Specific wear rate of bare CIPs and organosilane-coated CIPs based MRF with or without the presence of magnetic field.

or organosilane-coated CIPs (MRF-3APTS, MRF-HMDS, MRF-TEOS, MRF-VTMS). This reduction is attributed to the formation of a lubricating protective film and the rolling action of CIPs. These mechanisms collectively contribute to minimizing the direct metal-to-metal contact, thereby mitigating friction, as depicted in Fig. 7a. The introduction of a magnetic field led to an increase in the avg. COF, as depicted in Fig. 6. During off-state, the friction behaviour exhibits fluctuations due to the unrestricted movement of CIPs within the contact interface. Notably, the MRF containing bare CIPs (MRF-ES) demonstrated the highest COF value, possibly attributed to the abrasive nature of the CIPs. Furthermore, among the organosilane-coated CIPs, the HMDS-coated CIPs in particular displayed the lowest COF. This observation is ascribed to the formation of a thin tribo-layer in the contact interface, facilitating the removal of wear debris and easy sharing. Examining the COF in Fig. 6 (a1 and a2), it is evident that the COF of MRF-ES continuously increased with sliding time in both presence and absence of magnetic field. In contrast, MRFs utilizing organosilane-coated CIPs showed an initial increase in their COF, followed by a subsequent decrease over time in case of without magnetic field. This is attributed to the presence of sharp asperities initially requiring more lateral force. These sharp asperities become dull after sliding with the counter body due to the generation of wear particles and form a tribo-layer between the contact interface, which helps to maintain the stable COF afterwards as shown in Fig. 7 (b).

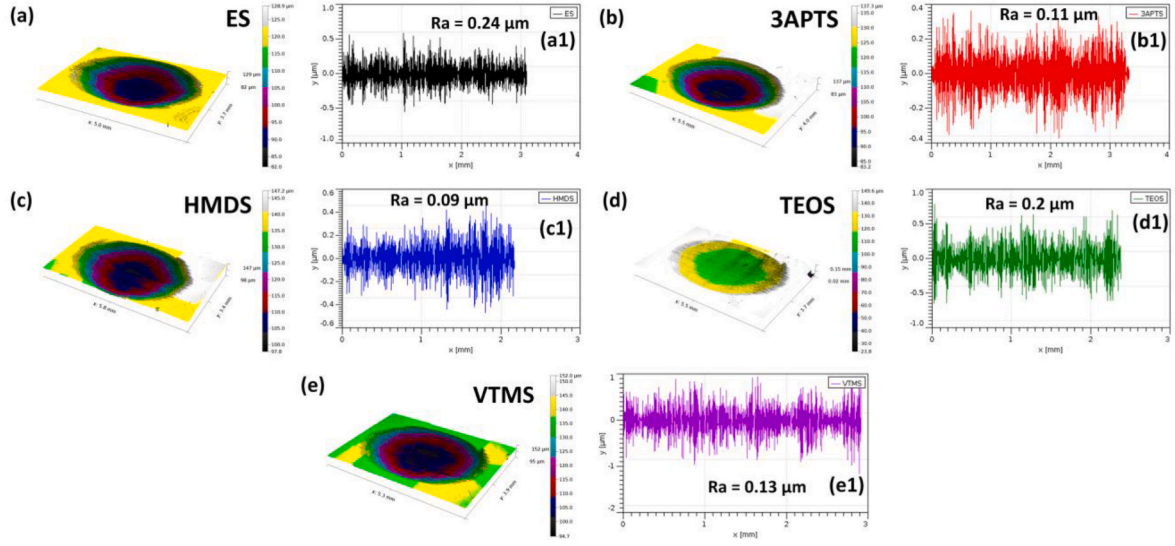

Fig. 10. (a–e) 3D profilometric images and (a1–e1) average roughness of the corresponding worn surfaces during the off-state.

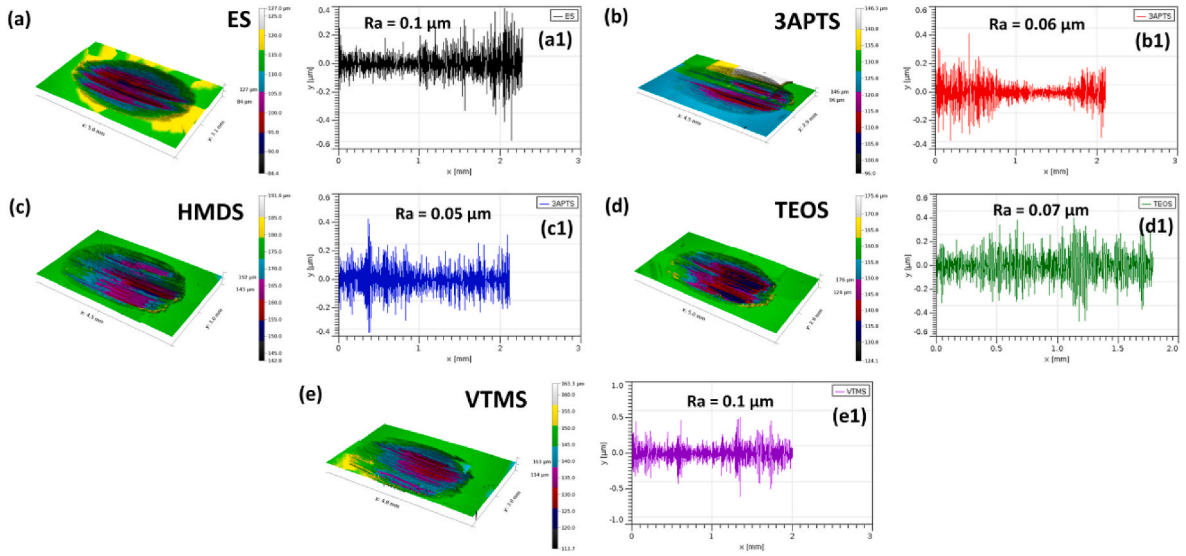

Fig. 11. (a–e) 3D profilometric images and (a1–e1) average roughness of the corresponding worn surfaces during the on-state.

However, within the magnetic field, the COF increased as the magnetic field strength increased. This rise in COF can be attributed to the formation of constraint chain which restricting the motion. As the sliding time increased, the outer layer of the organosilane-coated particles adhered to the contact interface, gradually thinning the coating layer. Consequently, the saturation of the CIP particles increased, leading to stronger magnetization, which further restricted motion and contributed to the increase in COF [50].

According to Peng et al. [51] the COF at the contact surface increased due to the formation of a constrained chain of iron particles aligned with the magnetic field.

The presence of a magnetic field, as depicted in Fig. 6, resulted in the increased COF. This phenomenon is ascribed to the attractive force among magnetic particles, resulting in the clustering of CIPs and an increase in the apparent viscosity due to the formation of a rigid chain-like structure of magnetic particles, as confirmed by (Fig. 3). Consequently, this raised the resistance to slide and contributed to the increase of the COF. Fig. 8(a) and (b) illustrate the schematic of the contact interface mechanism when the magnetic field is turned on and off, respectively.

Fig. 8b illustrates the formation of a chain during the alignment of the magnetic particles in the direction of the magnetic field, playing a crucial role in altering the COF [52,53]. The friction coefficient between the contact surfaces was increased as a result of the development of a rigid chain of iron particles oriented along the magnetic field direction [52,54]. Compared to MRF-ES, MRFs based on organosilane-coated CIPs showed a lower COF in the presence of a magnetic field. The friction behaviour was steady under field conditions due to the constrained chain formation of the CIPs in the contact interface, as presented in Fig. 6 (a2). Under the influence of the magnetic field, HMDS-coated surfaces exhibited a lower COF, possibly due to the creation of a mechanically mixed layer at the contact interface. A discernible difference was noted between the HMDS-coated and ES-based MRF. This suggests that organosilane coatings have a beneficial impact on reducing both the COF and wear when compared to the MRFs using bare CIPs. The inclusion of silica in the organosilanes (3-APTS, HMDS, TEOS, and VTMS) may contribute to the COF reduction by forming a solid protective layer at the contact interface [55–57].

Furthermore, the wear volume (with and without the presence of a magnetic field) was obtained from a 3D profilometer. The specific wear rate was then determined using Eq. (5) given as [58]:

$$\text{sp. wear rate} = \frac{W_v}{P \times S} \tag{7}$$

where W_v is the wear volume mm^3, P (N) is the applied load, and S is the sliding distance in (m).

The wear loss of the MRF with bare and organosilane-coated CIPs with and without magnetic field is presented in Fig. 9 in terms of sp. wear rate. The specific wear rate varies between (3.393×10^{-4} mm^3 N^{-1} m^{-1}) to (2.487×10^{-4} mm^3 N^{-1} m^{-1}) for the MRFs during the off-state. During the on-state, the sp. wear rate varies between (2.556×10^{-4} mm^3 N^{-1} m^{-1}) and (1.248×10^{-4} mm^3 N^{-1} m^{-1}), as shown in Fig. 9. The sp. wear rate was lower in the present of magnetic field. The sp. wear rate was analysed for various configurations, with MRF-ES exhibiting a sp. wear rate of 3.393×10^{-4} (mm^3 N^{-1} m^{-1}). When coated with 3APTS, HMDS, TEOS, and VTMS, the sp. wear rate decreased to 3.032×10^{-4}, 2.487×10^{-4}, 2.756×10^{-4} and 2.904×10^{-4} (mm^3 N^{-1} m^{-1}), respectively, as depicted in Fig. 9. Notably, all organosilane-coated CIPs demonstrated lower sp. wear rates compared to ES based MRF suspensions.

The lowest sp. wear rate was observed in MRF-HMDS (1.248×10^{-4} mm^3 N^{-1} m^{-1}), while the highest was seen in MRF-ES. This reduction in wear rate can be attributed to the formation of a mechanically mixed layer at the contact surfaces due to the organosilane coating on the CIPs particles. Specifically, the sp. wear rates for MRF-ES, MRF-3APTS, MRF-HMDS, MRF-TEOS, and MRF-VTMS were 2.556×10^{-4}, 2.121×10^{-4}, 1.248×10^{-4}, 1.708×10^{-4}, and 1.564×10^{-4} (mm^3 N^{-1} m^{-1}), respectively. Although slight differences were observed in the sp. wear rates among the various organosilanes, the MRF-ES exhibited the highest sp. wear rate under the influence of a magnetic field. The lower sp. wear rate in the presence of a magnetic field can be explained by the reduction in wear-scar dimensions. The influence of magnetic field on the concentration of the particles play a pivotal role, wherein the magnetic field lines promote particle concentration in specific regions.

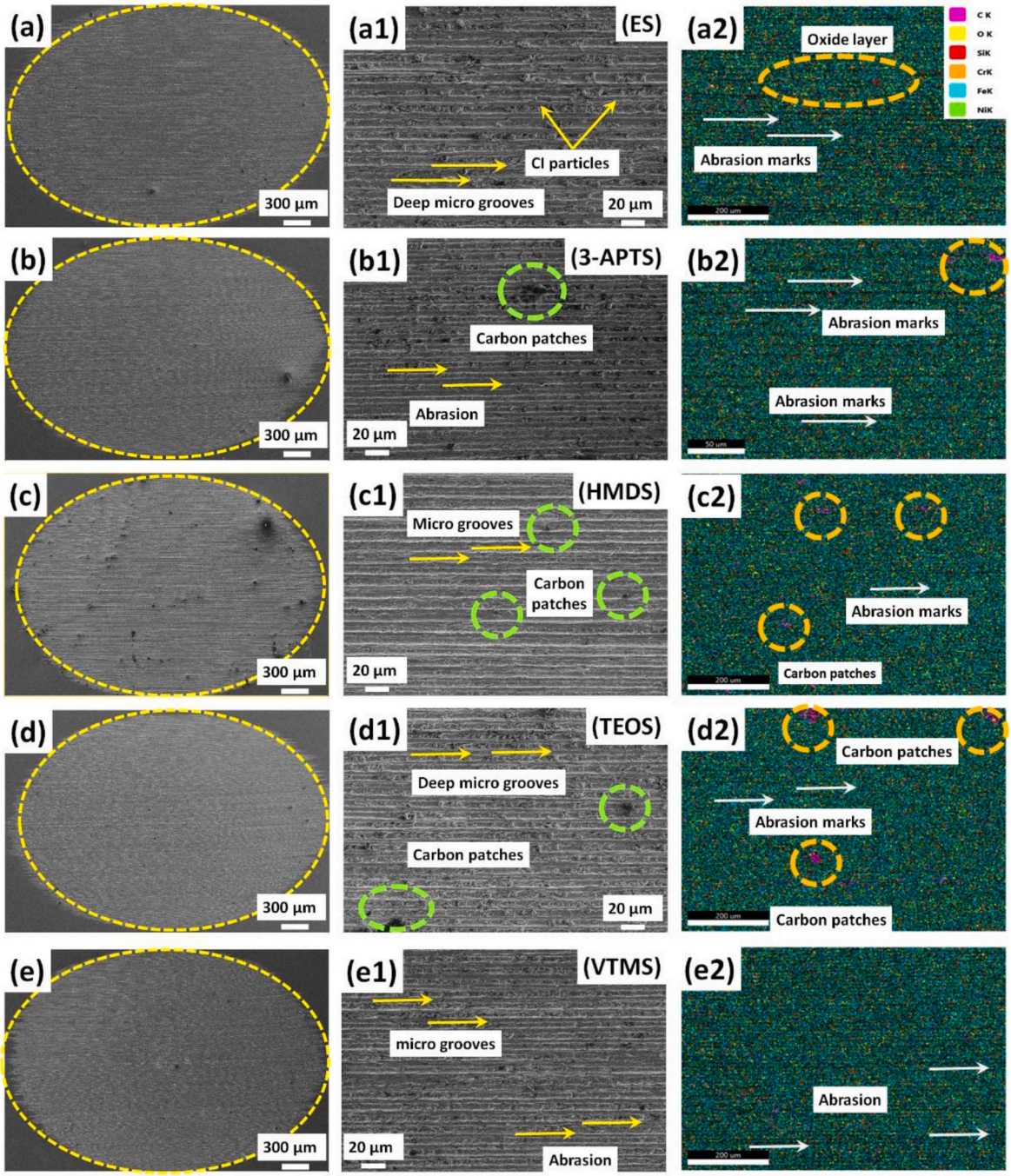

Fig. 12. FE-SEM of wear scars obtained for bare CIPs and organosilane-coated CIPs based MRF during the off-state.

This localized concentration restricts the abrasion region to a smaller zone, reducing wear-scar dimensions and consequently lowering sp. wear rates [46,58,59].

The specific wear rate observed in the MRF-ES and MRFs with various organosilane-coated CIPs (MRF-3APTS, MRF-HMDS, MRF-TEOS, MRF-VTMS) is in agreement with the results of the 3D profilometer. Fig. 10a–e and Fig. 11a–e depict that in the absence of the magnetic field, the average surface roughness was higher compared to when a magnetic field was present. Nonetheless, utilizing MRF with different organosilane-coated CIPs resulted in a lower roughness value when compared to MRF-ES. This aligns well with the COF since high COF is commonly correlated with the surface roughness (Ra) of the worn surface.

3.4.2. *Worn surface analysis*

The wear mechanism of the worn surfaces of the steel disc was analysed using FE-SEM and EDX. The investigation focused on the worn surface of the steel disc subjected to both bare CIPs and CIPs coated with organosilanes-based MRFs. EDX mapping provides insights into the presence of carbon, oxygen, and silicon on worn surfaces. Figs. 12 and 14 illustrate the FE-SEM analysis of the worn surfaces under both the absence and presence of an external magnetic field. The FE-SEM analysis revealed the wear mechanism, accompanied by abrasion, ploughing marks, and micro-grooves formation in the presence and absence of the magnetic field.

In the absence of a magnetic field, the examination of MRF-ES revealed the presence of deep microgrooves with some abrasive marks, as depicted in Fig. 12 (a and a1). The finding was further

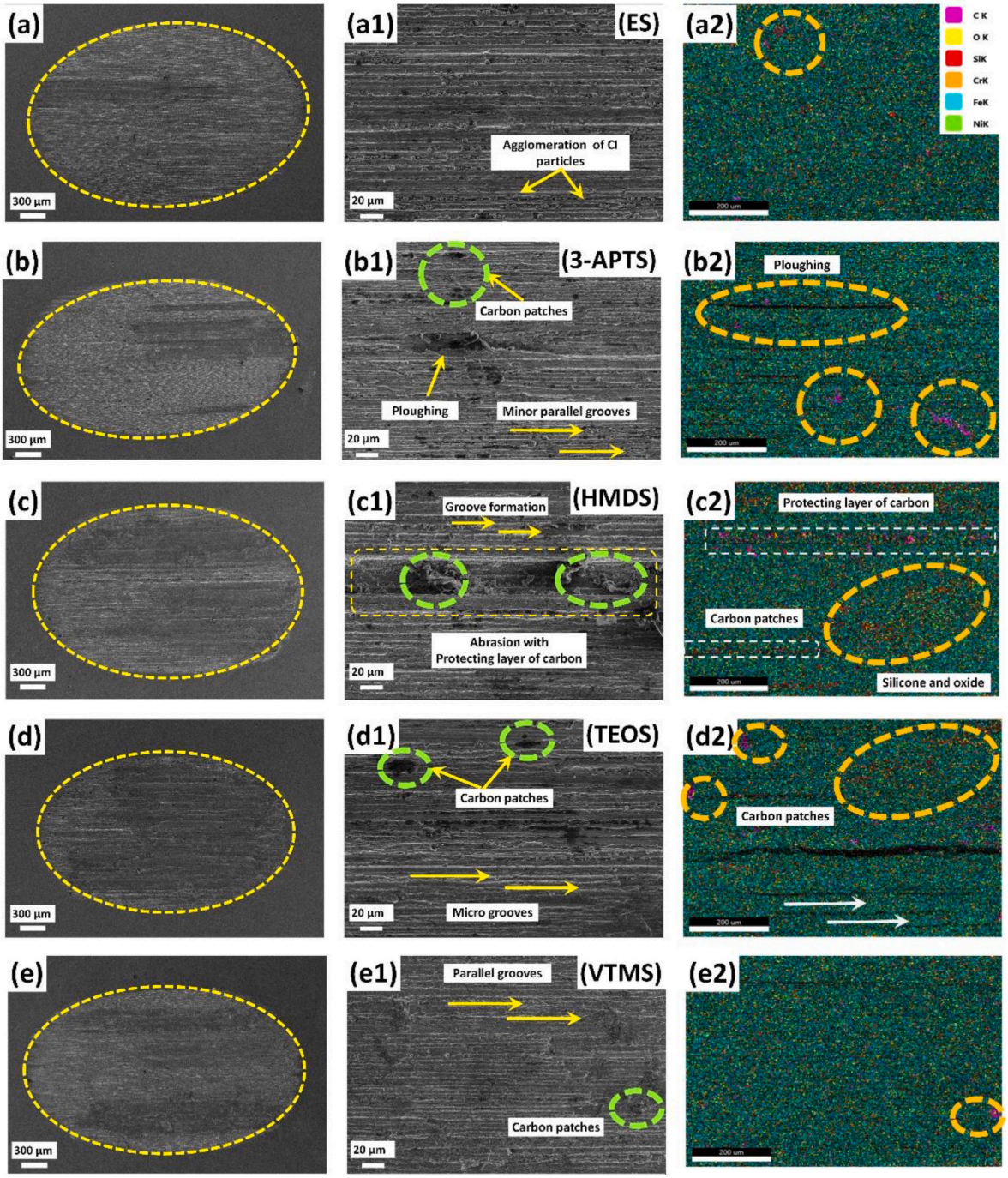

Fig. 13. FE-SEM of wear scars obtained for bare CIPs and organosilane-coated CIPs based MRF during the on-state.

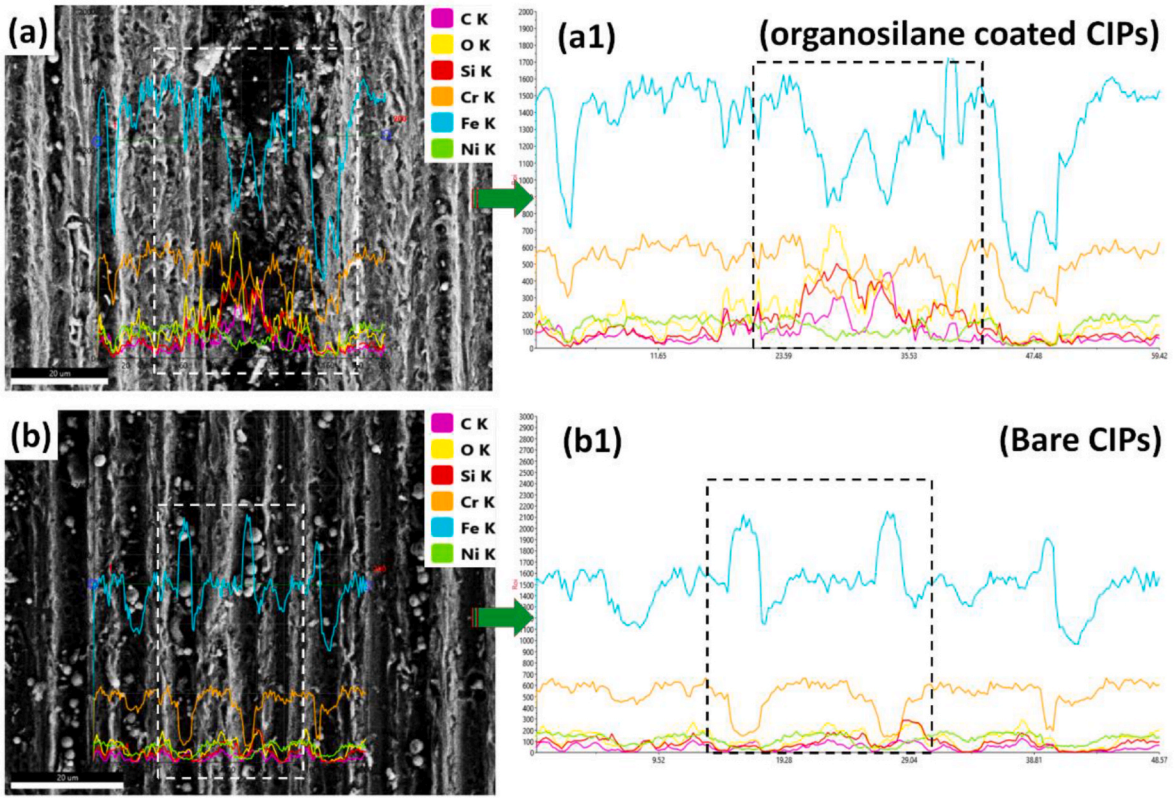

Fig. 14. EDX line mapping of wear scar of (a) organosilane-coated CIPs, and (b) bare CIPs based MRFs.

confirmed by EDX mapping as shown in Fig. 12 (a2) and Fig. S1 (supporting information). Conversely, MRFs based on organosilane-coated CIPs (3APTS, HMDS, TEOS, and VTMS) displayed only slight abrasion with some carbon patches, as illustrated in Fig. 12 (b, b1 & b2) to (e, e1 & e2). This is attributed to the organosilane coating layer over the CIPs, which diminished the abrasive nature of CIPs. The coating layer reduces the abrasive nature of CIPs and forms a protective layer at the contact interface. This protective layer contributes to an overall reduction in wear [60,61] of the MRF-HMDS and MRF-TEOS resulting in minor abrasive marks and microgrooves with some carbon patches on the worn surface.

In the presence of the magnetic field, a notable reduction in the size of the wear scar was observed compared to the wear scar obtained in the absence of a magnetic field. The MRF-ES showed minor grooves and agglomeration of the CIPs, along with some carbon patches which were evident on the contact surface under the magnetic field condition, as illustrated in Fig. 13 (a, a1 & a2).

In contrast, MRF with organosilane-coated CIPs results in microcracks with a protecting layer and carbon, silicon and oxygen patches, as depicted in Fig. 13 (b, b1 & b2) to (e, e1 & e2). This difference in wear characteristics is attributed to the protective layer (mechanically mixed layer) formed by the organosilane coating and the development of a constrained chain. These protective layers of organosilane coating significantly reduced the possibility of the CIPs entering the contact zone, thereby effectively diminishing wear [12]. EDX dot mapping in Fig. S2 (Supporting information) confirmed the presence of carbon patches and silicon, providing additional insights into the composition of the contact surface. For a more in-depth examination of the worn surface analysis and the reduction in wear, an EDX line mapping was utilized, as illustrated in Fig. 14 (a & b).

In Fig. 14 (a & a1), clear observations indicate that in the case of organosilane-coated CIPs, the intensity of iron (Fe), nickel (Ni), and chromium (Cr) elements is reduced, while other elements such as carbon (C), oxygen (O), and silicon (Si) exhibit higher levels, indicative of the formation of a protective film. Conversely, in Fig. 14 (b & b1) for bare CIPs (MRF-ES), the presence of carbon (C), oxygen (O), and silicon (Si) is diminished, while the intensity of iron (Fe), nickel (Ni), and chromium (Cr) elements are elevated. Based on this observation, it can be concluded that organosilane-coated CIPs decrease the COF and contribute to the reduction of wear.

The presence of oxygen (O), silicon (Si), and carbon (C) within the wear scar of HMDS-based MRF (Fig. 15) provides evidence for the formation of a mechanically mixed layer. This layer is notably more substantial than for other organosilane-coated particles, as indicated by the higher concentrations of Si, O, and C. The mechanically mixed layer plays a crucial role in the decreasing of the COF and wear. Fig. 16 depicts a schematic representation of the tribo-oxide formation during the wear process. Upon contact between the two surfaces, their micro asperities come into contact, facilitated by load application, leading to temporary welding of these asperities. However, the relative motion causes the breaking of these welded asperities. Initially, the broken asperities are sharp and irregular, but continuous load and relative motion leads to their dulling as they grind against each other to form dull wear debris. With ongoing load application and the generation of frictional heat, these wear debris agglomerate and eventually form a tribo-oxide layer. In this context, the CIPs become entrapped in the surface valleys, sliding

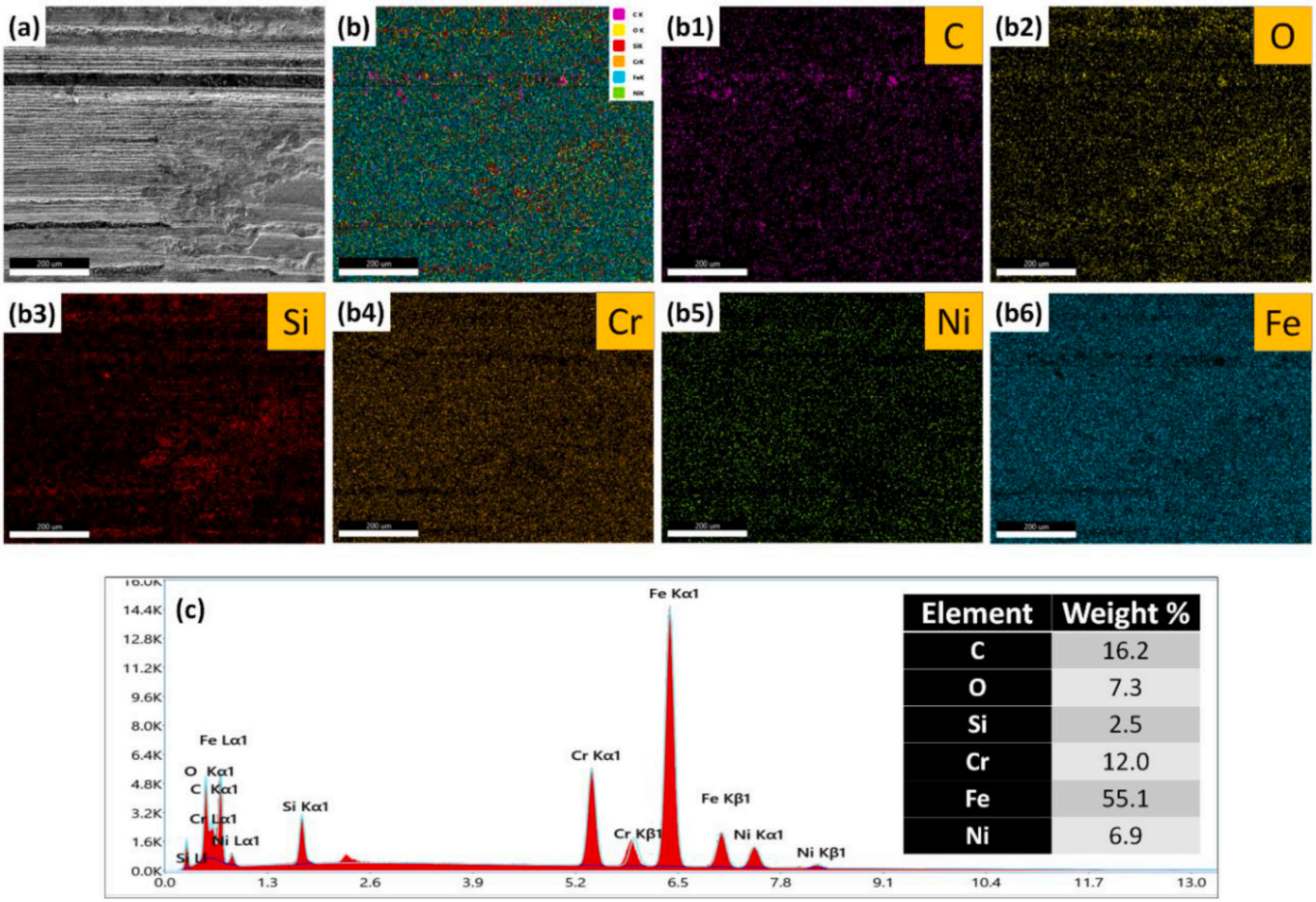

Element	Weight %
C	16.2
O	7.3
Si	2.5
Cr	12.0
Fe	55.1
Ni	6.9

Fig. 15. EDX images of the full scar obtained from MRF-HMDS.

along with the wear debris. The presence of organosilane coating on the CIPs facilitates the formation of a mechanically mixed layer on the surface. This layer acts as a protective barrier or film, reducing the COF and wear [62].

Lastly, Raman spectroscopy provided additional confirmation of the formation of the protective film comprising various organosilanes, as depicted in Fig. 17. The characteristic peaks identified at (D) 1317 cm^{-1} and (G) 1583 cm^{-1} correspond to the unique C–C bonds of carbon. Moreover, the significant peaks observed at 214.9 cm^{-1} and 492.07 cm^{-1} are attributed to the A1g symmetry mode, while the smaller peaks at 271.28 cm^{-1}, 381 cm^{-1}, and 645.89 cm^{-1} align with the Eg symmetry mode [63–66]. The presence of these peaks indicates the existence of ferrous oxide (Fe–O) at the interface of the contacts. Raman analysis reveals the presence of D and G bands of carbon, along with certain iron oxide bands, confirming the formation of this mechanically mixed layer at the contact surface. Conversely, other organosilane coatings show a lesser formation of the mechanical mixed layer, as evidenced by the absence or reduced intensity of D and G bands in the Raman spectra. This observation aligns well with the results obtained from the EDX analysis. The correlation between Raman spectroscopy and EDX analysis further strengthens the understanding of the formation and impact of the mechanically mixed layer on reducing wear and the COF in HMDS-based MRF compared to other formulations.

To conclude, it can be seen that three silanes (APTES, TEOS and VTMS) have relatively the same tribological properties or at least the trend between these was not clear. The main role is played by the modification bond, which in this case is Si–O–Fe. On the other hand, in case of HDMS, there is a direct Si–C–Fe bond and it could be more sustainable and provide better tribological performance.

4. Conclusions

This study explores the tribological characteristics of MRFs, analyzing various factors influencing system wear. The findings indicate that MRFs containing organosilane-coated CIPs generally exhibited lower viscosity compared to those with uncoated CIPs. Friction behavior was also influenced by the presence of the magnetic field. The COF was lower when no magnetic field was applied, with MRF-HMDS exhibiting a lower COF than MRF-ES. This trend was consistently observed across all MRFs containing organosilane-coated CIPs. These results highlight the potential advantages of using coated CIPs in MRF-based mechanical systems such as brakes and clutches, where high friction and minimal wear are crucial for performance and longevity. The wear characteristics of the system also improved with the introduction of organosilane-coated CIPs. The specific wear rate was notably lower in the presence of a magnetic field, demonstrating the effectiveness of coating in reducing material loss during operation. Additionally, the wear scar size significantly decreased with organosilane-coated CIPs, with a more pronounced reduction when a magnetic field was applied. The predominant wear mechanisms observed were three-body abrasion and parallel micro-groove formation, indicating that the coatings influenced the wear pattern of the system. Based on these findings, it can be concluded that organosilane-coated CIPs effectively reduce COF and wear on contact surfaces. Among the tested coatings, HMDS-coated CIPs exhibited the most substantial improvement, making them particularly promising for tribological applications requiring enhanced durability and performance.

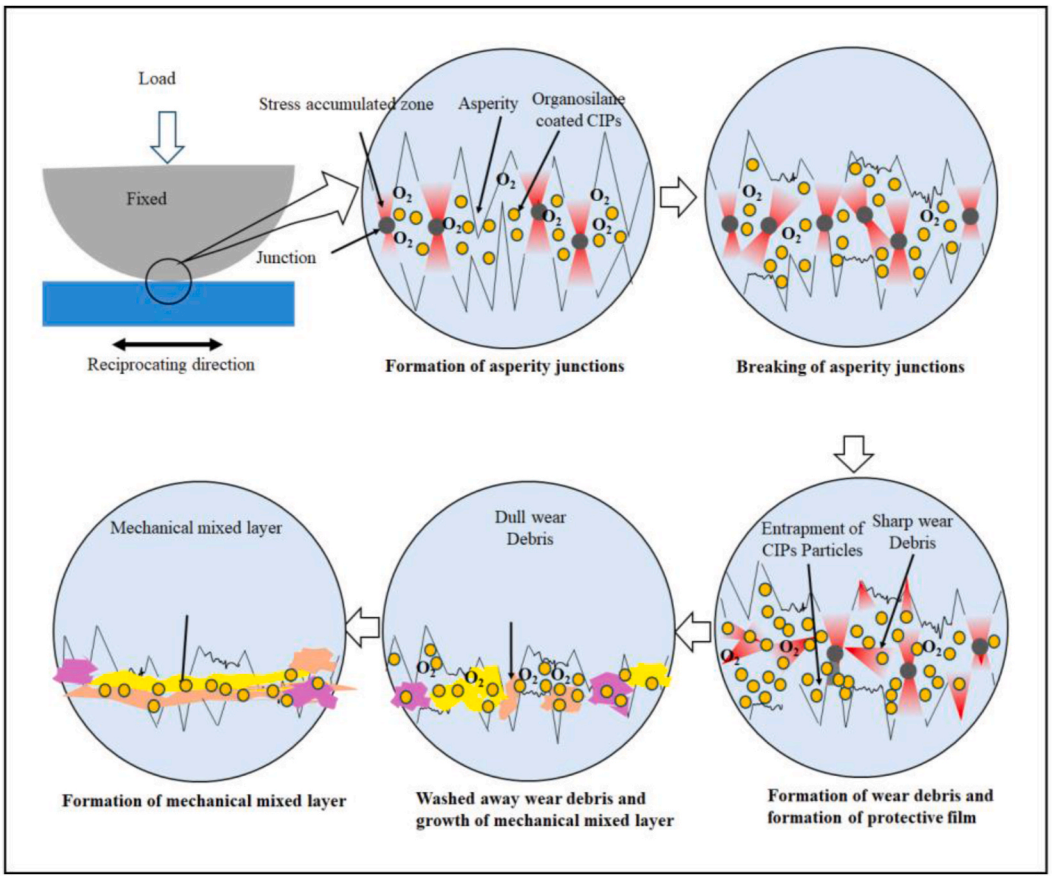

Fig. 16. Schematic of the formation of the mechanically mixed layer at the contact interface under MRF lubricating sliding condition.

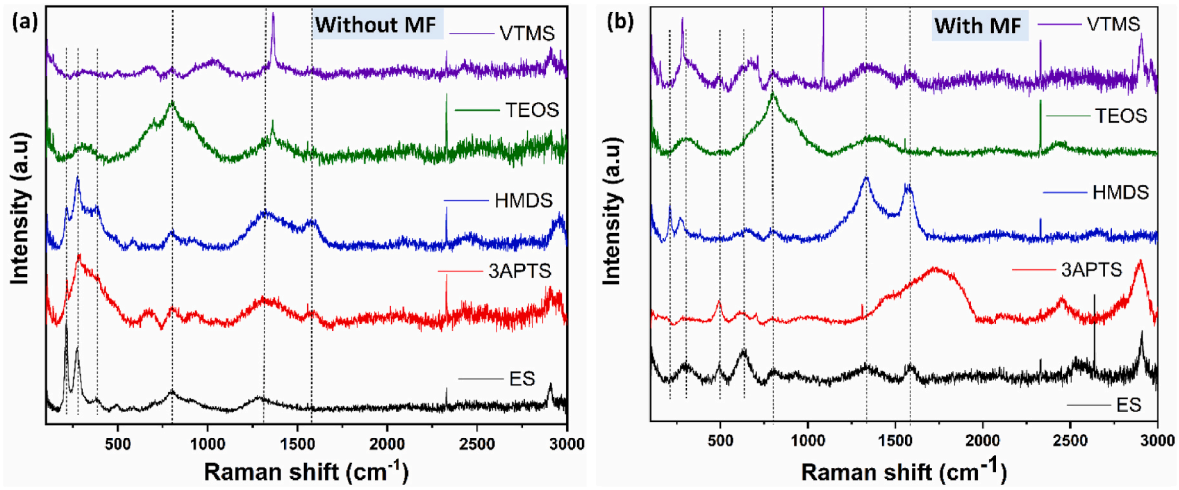

Fig. 17. Raman spectroscopy of worn-out surface for bare CIPs and organosilane coated CIPs based MRF (a) without magnetic field, (b) with magnetic field.

CRediT authorship contribution statement

Conceptualization: S. Kumar, R. Sehgal, M. Sedlacik; Methodology: M. Mrlik, M.F. Wani; Investigation: M. Kocak, S. Kumar, M. Mrlik, B. Kumar, C. Shekhar, P. Suly, M. Sedlacik; Writing – Original Draft: M. Kocak, S. Kumar, B. Kumar, C. Shekhar; Writing – Review & Editing: M. Mrlik, R. Sehgal, M.F. Wani, M. Kubik, M. Sedlacik; Visualization: S. Kumar, M. Mrlik, B. Kumar, C. Shekhar, M. Sedlacik; Supervision: R. Sehgal, M.F. Wani, M. Kubik, M. Sedlacik; Project administration: S. Kumar, M. Sedlacik, Funding acquisition: M. Kocak, M. Mrlik, M. Kubik, M. Sedlacik.

Data availability

Data will be made available on request.

Declaration of competing interest

The authors declare that they have no known competing financial interests or personal relationships that could have appeared to influence the work reported in this paper.

Acknowledgements

This work and the project were realized with the financial support of the internal grant of the TBU in Zlín no. IGA/FT/2025/004 funded from the resources of specific university research. The author Kubik M. wishes to thank the grant no. FSI–S-23-8212. The author Mrlik M. wishes to thank the DKRVO grant no. RP/CPS/2024-28/003 and author Sedlacik M. grant no. RP/CPS/2024-28/007.

Appendix A. Supplementary data

Supplementary data to this article can be found online at https://doi.org/10.1016/j.jmrt.2025.04.238.

References

[1] Bedi TS, Singh AK. An initial new approach for magnetorheological finishing of ferromagnetic internal cylindrical surfaces. Int J Adv Manuf Technol 2019;100:1017–30.
[2] Kumari C, Chak SK. A review on magnetically assisted abrasive finishing and their critical process parameters. Manuf Rev 2018;5:13.
[3] Mohd Nasir NA, Nazmi N, Mohamad N, Ubaidillah U, Nordin NA, Mazlan SA, Abdul Aziz SA, Shabdin MK, Yunus NA. Rheological performance of magnetorheological grease with embedded graphite additives. Materials 2021;14:5091.
[4] Ubaidillah J Sutrisno, Purwanto A, Mazlan SA. Recent progress on magnetorheological solids: materials, fabrication, testing, and applications. Adv Eng Mater 2015;17:563–97.
[5] Olabi A-G, Grunwald A. Design and application of magneto-rheological fluid. Mater Des 2007;28:2658–64.
[6] De Vicente J, Klingenberg DJ, Hidalgo-Alvarez R. Magnetorheological fluids: a review. Soft Matter 2011;7:3701–10.
[7] Yu J, Dong X, Zhang Z, Chen P. A novel scissor-type magnetorheological seat suspension system with self-sustainability. J Intell Mater Syst Struct 2019;30:665–76.
[8] Munteanu A, Plachý T, Munteanu L, Ngwabebhoh FA, Stejskal J, Trchová M, Kubík M, Sedlačík M. Bidisperse magnetorheological fluids utilizing composite polypyrrole nanotubes/magnetite nanoparticles and carbonyl iron microspheres. Rheol Acta 2023;62:461–72.
[9] Roupec J, Jeniš F, Strecker Z, Kubík M, Macháček O. Stribeck curve of magnetorheological fluid within pin-on-disc configuration: an experimental investigation. Materials 2020;13:4670.
[10] Yang J, Ning D, Sun SS, Zheng J, Lu H, Nakano M, Zhang S, Du H, Li WH. A semi-active suspension using a magnetorheological damper with nonlinear negative-stiffness component. Mech Syst Signal Process 2021;147:107071.
[11] Sarkar C, Hirani H. Effect of particle size on shear stress of magnetorheological fluids. Smart Sci. 2015;3:65–73.
[12] Hu ZD, Yan H, Qiu HZ, Zhang P, Liu Q. Friction and wear of magnetorheological fluid under magnetic field. Wear 2012;278:48–52.
[13] Wang N, Pang S, Ye C, Fan T, Choi S-B. The friction and wear mechanism of O-rings in magnetorheological damper: numerical and experimental study. Tribol Int 2021;157:106898.
[14] Li S, Xiu S, Song W, Sun C, Yang H. Research on the wear characteristics of magnetorheological fluid in sealing interface considering the interaction between surface roughness and magnetic particles. Tribol Int 2023;185:108496.
[15] Bombard AJF, de Vicente J. Boundary lubrication of magnetorheological fluids in PTFE/steel point contacts. Wear 2012;296:484–90.
[16] Chuah WH, Zhang WL, Choi HJ, Seo Y. Magnetorheology of core–shell structured carbonyl iron/polystyrene foam microparticles suspension with enhanced stability. Macromolecules 2015;48:7311–9.
[17] Kim YJ, Liu YD, Seo Y, Choi HJ. Pickering-emulsion-polymerized polystyrene/Fe_2O_3 composite particles and their magnetoresponsive characteristics. Langmuir 2013;29:4959–65.
[18] Shafrir SN, Romanofsky HJ, Skarlinski M, Wang M, Miao C, Salzman S, Chartier T, Mici J, Lambropoulos JC, Shen R. Zirconia-coated carbonyl-iron-particle-based magnetorheological fluid for polishing optical glasses and ceramics. Appl Opt 2009;48:6797–810.
[19] Jain VK, Sidpara A, Sankar MR, Das M. Nano-finishing techniques: a review. Proc Inst Mech Eng Part C J Mech Eng Sci 2012;226:327–46.
[20] Eshgarf H, Nadooshan AA, Raisi A. An overview on properties and applications of magnetorheological fluids: dampers, batteries, valves and brakes. J Energy Storage 2022;50:104648.
[21] Shahrivar K, Ortiz AL, de Vicente J. A comparative study of the tribological performance of ferrofluids and magnetorheological fluids within steel–steel point contacts. Tribol Int 2014;78:125–33.
[22] Zhang Y, Jiang J, Ouyang C, Meng Y, Jia W, Ma L, Tian Y. Effect of base oil lubrication properties on magnetorheological fluids. Smart Mater Struct 2021;30:95011.
[23] Michalec M, Svoboda P, Krupka I, Hartl M. Tribological behaviour of smart fluids influenced by magnetic and electric field—a review. Tribol. Ind. 2018;40:515–28.
[24] Upadhyay RV. Steady shear rheology and magnetic properties of flake-shaped iron particle-based MR fluid: before and after tribology study. Braz J Phys 2019;49:820–8.
[25] Upadhyay RV, Laherisheth Z, Shah K. Rheological properties of soft magnetic flake shaped iron particle based magnetorheological fluid in dynamic mode. Smart Mater Struct 2014;23:015002.
[26] Shilan ST, Mazlan SA, Ido Y, Hajalilou A, Jeyadevan B, Choi SB, Yunus NA. A comparison of field-dependent rheological properties between spherical and plate-like carbonyl iron particles-based magneto-rheological fluids. Smart Mater Struct 2016;25:095025.
[27] Zhang WL, Qu F, Tian Y, Choi HJ, Deng L, Liu J, Tian J, Liu H. Elegant surface of CoNi alloys toward efficient magnetorheological performances realized with carbon quantum dots. Adv Mater Interfac 2018;5:1800164.
[28] Ghasemi SS, Ebrahimi NG, Hajalilou A. Simultaneous effect of magnetic nanoparticles additive and noble metal coating on carbonyl iron-based magnetorheological fluid. J Alloys Compd 2023;961:171012.
[29] Hajalilou A, Kianvash A, Shameli K, Lavvafi H. Carbonyl iron based magnetorheological effects with silver nanoparticles via green-assisted coating. Appl Phys Lett 2017;110:261902.
[30] Singh RK, Sarkar C. Study of effect of graphite-based magnetorheological fluids on braking performance and rotor surface of magnetorheological disk brake using full-scale brake inertia dynamometer. Tribol Trans 2024;67:1–16.
[31] Song W, Wang S, Choi S-B, Wang N, Xiu S. Thermal and tribological characteristics of a disc-type magnetorheological brake operated by the shear mode. J Intell Mater Syst Struct 2019;30:722–33.
[32] Juretzka B, Wieber S, Wilkens R, Hagemann M, Kolb R, Riedel R. Tribological behavior of film-forming organosilane/-siloxane oil additives: film characterization and influences on lubrication. Tribol Lett 2019;68:5.
[33] Satyanarayana N, Sinha SK, Srinivasan MP. Friction and wear life evaluation of silane-based self-assembled monolayers on silicon surface. Tribol. Interface Eng. Series 2005;16:821–6.
[34] Yamaura M, Camilo RL, Sampaio LC, Macêdo MA, Nakamura M, Toma HE. Preparation and characterization of (3-aminopropyl) triethoxysilane-coated magnetite nanoparticles. J Magn Magn Mater 2004;279:210–7.
[35] Li YZ, Li Z, Gao Y, Li L, Yang YH. Influences of (3-aminopropyl)triethoxysilane on the tribological behaviors of basalt fiber/acrylonitrile-butadiene rubber composites under dry friction and water-lubricated conditions. J Appl Polym Sci 2020;137:9.
[36] Halford J, Chen CF. The role of APTES as a primer for polystyrene coated AA2024-T3. Micromachines 2024;15:17.
[37] Wang L, Lei XL, Shen B, Sun FH, Zhang ZM. Tribological properties and cutting performance of boron and silicon doped diamond films on Co-cemented tungsten carbide inserts. Diam Relat Mater 2013;33:54–62.
[38] Ronzova A, Sedlacik M, Cvek M. Magnetorheological fluids based on core–shell carbonyl iron particles modified by various organosilanes: synthesis, stability and performance. Soft Matter 2021;17:1299–306.
[39] Bandl C, Krempl N, Berger-Weber G, Kern W, Friesenbichler W. Application of organosilane coatings for improved anti-adhesive properties enabling facilitated demolding in polymer processing. J Appl Polym Sci 2021;138:e50714.
[40] Ivashchenko VI, Porada OK, Ivashchenko LA, Timofeeva II, Sinel'nichenko OK, Butenko OO, et al. Characteristics of thin plasmachemical silicon carbon nitride films deposited using hexamethyldisilane. Powder Metall Met Ceram 2009;48:66–72.
[41] Figueroa NS, Nachez JL, Freire FL, Maia da Costa MEH. Synthesis and characterization of hexamethyldisilane films deposited on stainless steel by plasma-enhanced chemical vapour deposition. Surf. Coat. Technol. 2020;404:126443. https://doi.org/10.1016/j.surfcoat.2020.126443.
[42] Mrlik M, Ilcikova M, Sedlacik M, Mosnacek J, Peer P, Filip P. Cholesteryl-coated carbonyl iron particles with improved anti-corrosion stability and their viscoelastic behaviour under magnetic field. Colloid Polym Sci 2014;292:2137–43.
[43] Sedlacik M, Pavlinek V, Vyroubal R, Peer P, Filip P. A dimorphic magnetorheological fluid with improved oxidation and chemical stability under oscillatory shear. Smart Mater Struct 2013;22:035011.
[44] Hamrock BJ, Dowson D. Isothermal elastohydrodynamic lubrication of point contacts—3. Fully flooded results. Am Soc Mech Eng 1977;99:264–75.
[45] Raina A, Anand A. Tribological investigation of diamond nanoparticles for steel/steel contacts in boundary lubrication regime. Appl Nanosci 2017;7:371–88.
[46] Sakurai H, Hosomi A. Thermal Si-Si/Si-Si redistribution of hexaorganodisilane—new thermally forbidden molecular reaction. J Organomet Chem 1972;36:C15–7.
[47] Mrlík M, Ilcíková M, Cvek M, Pavlínek V, Zahoranová A, Kroneková Z, Kasak P. Carbonyl iron coated with a sulfobetaine moiety as a biocompatible system and the magnetorheological performance of its silicone oil suspensions. RSC Adv 2016;6:32823–30.
[48] Sedlacik M, Pavlínek V. A tensiometric study of magnetorheological suspensions' stability. RSC Adv 2014;4:58377–85.
[49] Zhang P, Dong YZ, Choi HJ, Lee C-H. Tribological and rheological tests of core-shell typed carbonyl iron/polystyrene particle-based magnetorheological fluid. J Ind Eng Chem 2018;68:342–9.

[50] Mehdizadeh A, Mei R, Klausner JF, Rahmatian N. Interaction forces between soft magnetic particles in uniform and non-uniform magnetic fields. Acta Mech Sin 2010;26:921–9.
[51] Peng Z, Lee KH, Lee CH. Friction behavior of magnetorheological fluids with different material types and magnetic field strength. Chinese J. Mech. Eng. (English Ed. 2016;29(1):84–90.
[52] Wong PL, Bullough WA, Feng C, Lingard S. Tribological performance of a magneto-rheological suspension. Wear 2001;247:33–40.
[53] Kumar S, Sehgal R, Wani MF, Sharma MD, Ziyamukhamedova U, Dar TA. Next-generation ecofriendly MR fluid: hybrid GO/Fe2O3 encapsulated carbonyl iron microparticles with improved magnetorheological, tribological, and corrosion resistance properties. Carbon 2023;214:118331.
[54] Petry ER, Boeira CD, Cemin F, Leidens LM, Bim LT, Larrude DG, Maia da Costa MEH, Figueroa CA. Physicochemical structure of SiCx to improve DLC adhesion on steel. Surf Eng 2016;32:779–85.
[55] Wei R, Rincon C, Langa E, Yang Q. Microstructure and tribological performance of nanocomposite Ti–Si–C–N coatings deposited using hexamethyldisilazane precursor. J Vac Sci Technol A 2010;28:1126–32.
[56] Karami P, Shojaei A. Effect of type of diamine modifiers of nanodiamond on tribo-mechanical properties of polyamide 6 composites. ICCM Int. Conf. Compos. Mater. August 2017:20–5.
[57] Shahrivar K, Ortiz AL, De Vicente J. A comparative study of the tribological performance of ferrofluids and magnetorheological fluids within steel-steel point contacts. Tribol Int 2014;78:125–33.
[58] Kumar B, Kumar D, Chaudhry V. Tribological behavior of zirconium alloy against stainless steel under different conditions. Tribol Int 2023;189:108995.
[59] Song WL, Choi SB, Choi JY, Lee CH. Wear and friction characteristics of magnetorheological fluid under magnetic field activation. Tribol Trans 2011;54:616–24.
[60] Figueroa NS, Nachez JL, Freire Jr FL, da Costa MEHM. Synthesis and characterization of hexamethyldisilane films deposited on stainless steel by plasma-enhanced chemical vapour deposition. Surf Coat Technol 2020;404:126443.
[61] Kumar S, Sehgal R, Wani MF, Sharma MD. Friction and wear properties of core-shell (CI as core & GO as shell) particles based magnetorheological fluid under steel on steel point contacts. J Ind Eng Chem 2023;118:446–57.
[62] Kumar B, Kumar D, Chaudhry V. Mechanism of wear in zircaloy-4 under different loading conditions. Tribol Int 2023;182:108369.
[63] Yadav A, Kumar R, Choudhary HK, Sahoo B. Graphene-oxide coating for corrosion protection of iron particles in saline water. Carbon 2018;140:477–87.
[64] Fleischer K, Mauit O, Shvets IV. Stability and capping of magnetite ultra-thin films. Appl Phys Lett 2014;104:192401.
[65] Rinnert H, Vergnat M, Burneau A. Evidence of light-emitting amorphous silicon clusters confined in a silicon oxide matrix. J Appl Phys 2001;89:237–43.
[66] Borowicz P, Taube A, Rzodkiewicz W, Latek M, Gierałtowska S. Raman spectra of high-κ dielectric layers investigated with micro-Raman spectroscopy comparison with silicon dioxide. Sci World J 2013:208081.